J Porous Mater (2015) 22:705–711
DOI 10.1007/s10934-015-9943-7

Preparation and characterization of mesostructured Zr-SBA-16: efficient Lewis acidic catalyst for Hantzsch reaction

Rajamanickam Maheswari[1] · Vinju Vasudevan Srinivasan[1] · Anand Ramanathan[2] · Muthusamy P. Pachamuthu[1] · Rajamanickam Rajalakshmi[1] · Gaffar Imran[1]

Published online: 17 March 2015

Abstract Mesostructured Zr-SBA-16 (3D cubic arrangement, *Im3m* space group) with different Si/Zr ratio was successfully synthesized by using Pluronic F127 triblock copolymer and *n*-butanol as a structure directing agent. Successful incorporation of Zr^{4+} ions was achieved without any pH adjustments up to ~6.5 wt% of Zr loading. Different analytical techniques such as SAXS, N_2-physisortion and HR-TEM were used to ascertain the structure of Zr-SBA-16 samples whereas, diffuse reflectance UV–Vis, pyridine adsorbed FTIR and NH_3 desorbed TPD methods were assessed to understand the nature of Zr incorporation. The Lewis acidity of Zr-SBA-16 was explored in the synthesis of Hantzsch 1,4-dihydropyridine derivatives via condensation of substituted benzaldehyde, ethyl acetoacetate and ammonium acetate.

Keywords Amorphous materials · Zr-SBA-16 · Lewis acid · Hantzsch reaction

1 Introduction

Mesoporous silicates based solid acids are gaining importance as catalysts for transformation of biomass based substrates [1, 2]. Among them, the most studied mesoporous supports were MCM-41 and SBA-15 (possessing one-dimensional hexagonal mesoporous), due to their relative ease and wide range of synthesis co nditions [3, 4]. On the other hand, studies on catalysis using metal incorporated/functionalized SBA-16, a cubic mesoporous silicate with *Im3m* space group [5] was found limited due to its narrow range of synthesis conditions [6]. In addition, the pH of the synthesis gel was adjusted to incorporate catalytic species such as V [7], Cu [8] and Ti [9].

We have recently shown that the metal ions such as W [10] and Nb [11] can be incorporated effectively into SBA-16 without any significant adjustments to the synthesis condition reported by Kleitz et al. [5]. The incorporation of transition metal ions, in general, creates Lewis acid sites in mesoporous materials. For instance, W- and Nb- incorporated SBA-16 [10, 11] showed Lewis acid sites that are responsible for epoxidation activity, however, Brønsted sites were unfavorable for selectivity toward epoxide [11, 12]. Recently, Al incorporation was achieved by direct synthesis method on to SBA-16 silicate and their acid sites were characterized by CO adsorbed FTIR spectra [13]. It is suggested again that high Al content can be achieved by adjusting pH. Zr^{4+} and Sn^{4+} ions were framework substituted in SBA-16 by the microwave synthesis method and are shown to be active for Lewis acid catalyzed reactions such as Meerwein–Ponndorf–Verly reduction of cyclohexanone and Baeyer–Villiger oxidation of adamantanone [14].

In this regard, we intend to extend our direct synthesis strategy to incorporate Zr into SBA-16 silicate with different Zr loading. Depending on the loading, the Lewis acidity of the materials were varied and are shown to be effective for the condensation synthesis of DHP.

2 Experimental

2.1 Synthesis of Zr-SBA-16

The Zr-SBA-16 with varying Si/Zr atomic ratio (100, 50 and 25) samples was prepared under acidic conditions

✉ Rajamanickam Maheswari
maheswarianand@annauniv.edu

[1] Department of Chemistry, Anna University, Chennai 600025, India

[2] Center for Environmentally Beneficial Catalysis, The University of Kansas, Lawrence, KS 66047, USA

similar to our previous reports of Nb- and W-SBA-16 [10, 11]. In a typical synthesis, 3.5 g of F127 ($EO_{106}PO_{70}EO_{106}$, Sigma Aldrich) and 175 mL of 0.4 M HCl solution were mixed in a polypropylene bottle to obtain a homogeneous solution at 45 °C. To this, 13 mL of *n*-butanol (Acros Organics) was added and continued stirring for approximately 60 min. Finally a mixture of tetraethyl orthosilicate (TEOS, 98 %, Sigma Aldrich) and zirconyl chloride octahydrate ($ZrOCl_2{\cdot}8H_2O$, Sigma Aldrich) were added. After stirring for another 20 h, the mixture is then heated at 98 °C for another 24 h in a static oven. The as-synthesized Zr-SBA-16 was then filtered and dried at 100 °C. Template free Zr-SBA-16 was obtained by calcination of the as-synthesized sample in a flow of air at 550 °C for 5 h at a heating rate of 1.5 °C/min. The resulting solids are indicated as Zr-SBA-16 (Si/Zr atomic ratio).

2.2 Characterization

Powder XRD patterns were recorded in Phillips X′pert X-ray diffractometer with Cu-Kα radiation ($\lambda = 0.1548$ nm) in the range of 0.5–5° and 10–80° 2θ value. The specific surface area, pore size distribution and pore volume was evaluated from N_2 physisorption method using Micromeritics ASAP 2020 porosimeter system at liquid nitrogen temperature. The amount of Zr incorporated in the final solid was analyzed by inductively coupled plasma optical emission spectroscopy (ICP-OES) on a Perkin Elmer OES Optima 5300 DV spectrometer. The nature of Zr incorporation was evaluated from diffuse reflectance UV–Vis (Thermo scientific Evolution 600) spectrometer with a diffuse reflectance attachment, using $BaSO_4$ as the reference. FTIR spectra of KBr-diluted pellets of the sample were recorded on a Bruker instrument at room temperature with a resolution of 4 cm^{-1} averaged over 100 scans. Transmission electron microscopy measurement for the reduced catalysts was carried out in JEOL 200 kV electron microscope operating at 200 kV. Pyridine FTIR spectra of the samples were carried out by mixing pyridine with sample and dried it 120 °C in atmospheric pressure analyzed in the DRIFT mode in the FTIR instrument. The X-ray photoelectron spectroscopy (XPS) spectra were carried out by using a Physical Electronics PHI 5800 ESCA system with standard non-monochromatic Al Kα X-rays (1486.6 eV) operated at 250 W and 15 kV. The Temperature programmed desorption of ammonia (NH_3-TPD) were carried out on a ChemBET TPD/TPR instrument equipped with a thermal conductivity detector (TCD) [15]. Briefly, about 30 mg of the catalyst has been loaded into U-shaped quartz tube and was activated under N_2 (80 cm^3/min) atmosphere for 2 h at 200 °C with the ramp of 40 °C/min. Then it was cooled to 100 °C and ammonia was adsorbed using 10 % NH_3/90 % He mixture and the ammonia desorbed was monitored between 100 and 550 °C with a flow rate of 60 cm^3/min and at the ramp of 10 °C/min.

2.3 Catalytic activity

For the Hantzsch reaction, freshly distilled benzaldehyde (1 mmol), ethyl acetoacetate (2 mmol), ammonium acetate (1.2 mmol) 4 ml of ethanol (solvent) and Zr-SBA-16 (containing 0.06 mmol Zr), catalyst were added to a 25 mL two neck round bottom flask equipped with a condenser and magnetic stir bar. The reaction was started by immersing the flask into preheated oil bath at 80 °C and was monitored by TLC (monitored using hexane: ethyl acetate 7:3). After completion of the reaction, the resultant mixture was cooled down to room temperature, filtered (to separate the catalyst) and the filtrate was added to cold water and the formed precipitate was filtered off. The crude product was further purified by recrystallization using ethanol. The isolated pure compound was confirmed by ^{1}H·NMR, ^{13}C·NMR and FT-IR (not shown) and also by comparison with the literature reports [16, 17].

3 Results and discussions

Figure 1a illustrates the low angle powder XRD patterns of Zr-SBA-16 samples which displayed three reflections at $2\theta = 0.77°$, 1.33° and 1.56° indexed to (110), (200) and (211) diffractions respectively typically of cubic *Im3m* structure. No significant changes in the intensity or position of d_{111} plane was observed with Zr loading. The average unit cell parameter (calculated using $a_0 = d_{110}\sqrt{2}$) is given in Table 1 and are observed very close to SBA-16 reported by us earlier [10]. Further, ICP-OES analysis of Zr-SBA-16 samples revealed a close Si/Zr ratio that of synthesis gel, suggesting that all of Zr is incorporated in the final SBA-16 solids. However, in the high angle XRD (Fig. 1b) no peak responsible for crystalline ZrO_2 was noticed indicating that Zr is either framework incorporated or homogeneously dispersed as amorphous ZrO_2 nanoparticles. The hump observed between $2\theta = 15–30°$ is due to amorphous nature of silica network.

The N_2 adsorption–desorption isotherms and pore size distribution of Zr-SBA-16 samples are depicted in Fig. 2a, b respectively. The structural parameters derived from the N_2 isotherm is given in Table 1. All Zr-SBA-16 showed type IV with H_2 hysteresis characteristic of mesoporous materials with large uniform cage-type porosity, according to the IUPAC classification [10, 11]. Zr-SBA-16 samples also presented higher surface area and pore volume compared to SBA-16. Notably, area of micropores decreased with increase in Zr loading, suggesting that some ZrO_2 may

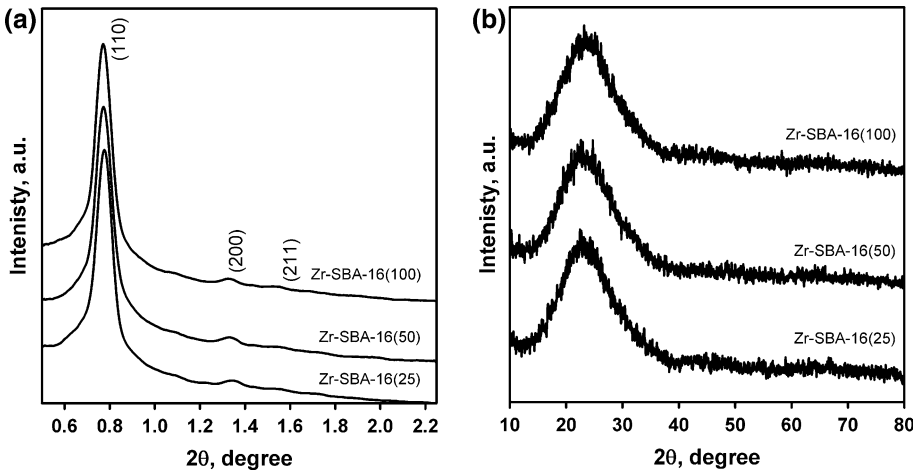

Fig. 1 **a** Low angle XRD and **b** high angle XRD of Zr-SBA-16 samples

Table 1 Physico-chemical characteristics of Zr-SBA-16 samples with different Zr contents

SBA-16 (Si/Zr)[a]	Si/Zr[b]	Zr (wt%)	a_0^c (nm)	S_{BET}^d (m^2/g)	A_{mp}^e (m^2/g)	V_{rp}^f (cc/g)	V_{mp}^g (cc/g)	$d_{P,\ NLDFT}^h$ (nm)	Total acidity (mmol NH_3/g)
SBA-16	∞		16.2	796	340	0.69	0.17	9.4	0.02
Zr-SBA-16(100)	93	1.6	16.2	1012	491	0.82	0.22	9.7	0.21
Zr-SBA-16(50)	45	3.2	16.0	984	470	0.78	0.21	9.7	0.34
Zr-SBA-16(25)	22	6.5	15.6	1022	223	0.91	0.1	9.9	0.55

[a] Molar ratio in the synthesis gel

[b] Actual molar ratio in sample determined by ICP-OES

[c] a_0 unit cell parameter ($a_0 = d_{111}\sqrt{3}$)

[d] S_{BET} specific surface area determined using Brunauer–Emmett–Teller (BET) equation from adsorption isotherm at P/P_0 between 0.05 and 0.30

[e] A_{mp} micropore area estimated from t-plot method

[f] V_{rP} total pore volume at 0.98 P/P_0

[g] V_{mP} micropore volume estimated from t-plot method

[h] $d_{P,\ NLDFT}$ determined using NLDFT kernel developed for silica exhibiting cylindrical/spherical pore geometry

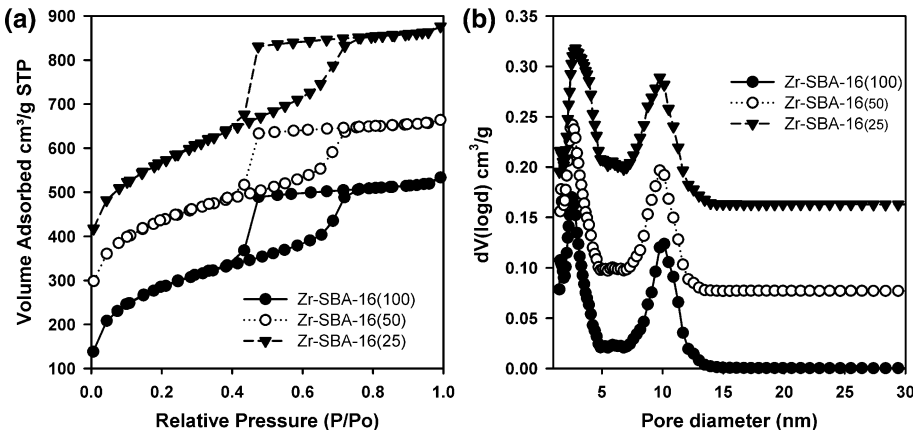

Fig. 2 **a** Nitrogen physisorption and **b** NLDFT pore size distributions of Zr-SBA-16 samples. The data in **a** are *vertically* shifted by 150 and 257 units respectively for Zr-SBA-16(50) and Zr-SBA-16(25)

be present as extra framework species. The pore size distribution curves obtained from NLDFT adsorption branch method confirm the presence of cage pores (~9.9 nm) with entrance pores between 2.5 and 2.9 nm similar to other SBA-16 type materials [10, 11]. The structural ordering is further verified from the high resolution TEM

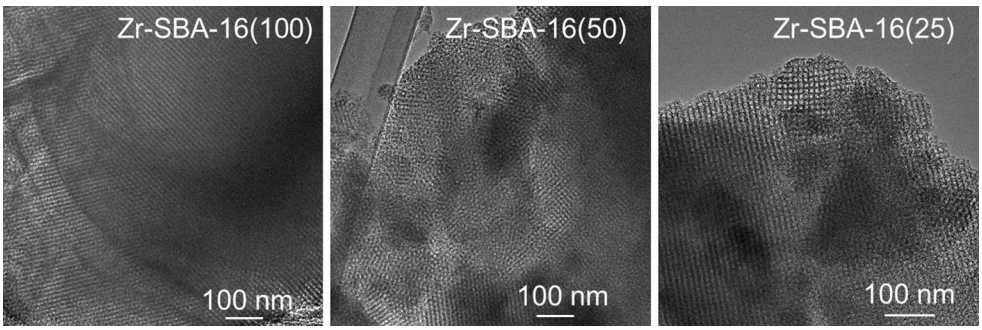

Fig. 3 High resolution TEM images of Zr-SBA-16 samples

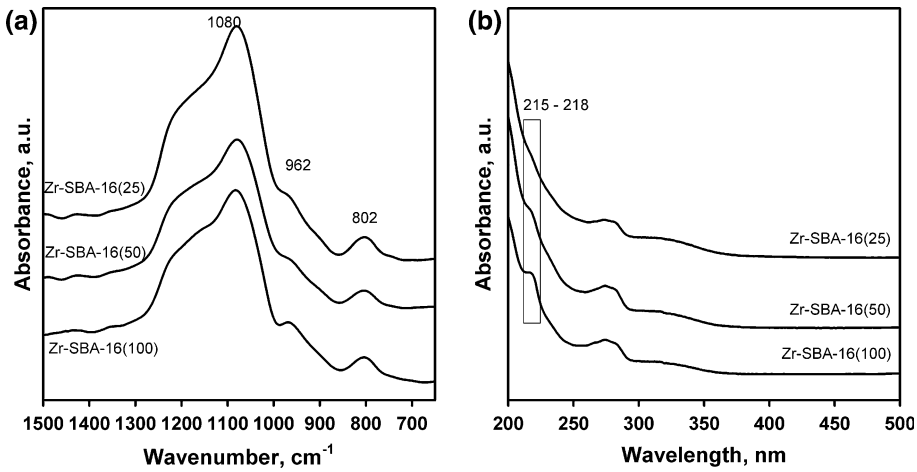

Fig. 4 **a** FTIR spectra of KBr diluted Zr-SBA-16 samples in the skeletal region and **b** diffuse reflectance UV–Vis of Zr-SBA-16 samples

images of Zr-SBA-16 (Fig. 3) displaying periodic arrangement of cubic type pores over very large areas typically observed for SBA-16 type materials [10, 11].

FTIR spectra of KBr diluted Zr-SBA-16 samples are given in Fig. 4a. The peaks observed around 1080 and 802 cm^{-1} are assigned to asymmetric and symmetric vibrations of Si–O–Si linkages respectively. The band near 960 cm^{-1} is assigned to the Si–O–H and/or Si–O–Zr stretching vibration indicating the framework incorporation of Zr ions [18, 19]. Further, Zr-incorporation is verified from diffuse reflectance UV–Vis (Fig. 4b). All Zr-SBA-16 samples displayed a peak around 215–218 nm corresponding to O → Zr^{4+} charge transfer transitions in tetrahedral coordination [19–24]. In addition existence of ZrO_2 nanoparticles that are homogeneously distributed was evidenced from 280 nm peak [19–24].

The acidity of Zr-SBA-16 samples is measured in the temperature range 100–550 °C by NH_3-TPD and the results are shown in Fig. 5a and Table 1. While the acidity of SBA-16 was only 0.02 mmol NH_3/g [10], with increasing Zr loading, ammonia desorption increased and thus the total acidity of Zr-SBA-16 samples (0.21–0.55 mmol NH_3/g). These observation further indirectly suggest the incorporation of Zr species. Though the number of acid sites increased with Zr loading the nature of acid sites are observed similar as all Zr-SBA-16 samples desorb NH_3 in the similar range of temperature (150–400 °C). To differentiate Lewis (L) and Brønsted (B) acid sites in Zr-SBA-16 samples, FTIR spectra of adsorbed pyridine was studied and the results are presented in Fig. 5b. The absorption band at around 1440 cm^{-1} is typically of pyridine adsorbed on Lewis acid sites which increased with Zr content. The absorption band due to Brønsted acid sites is typically observed at 1540 cm^{-1} and the absence of this peak suggest that Zr-SBA-16 possessed predominantly Lewis acid sites similar to ZrTUD-1 and Zr-KIT-6 [22, 25]. The combination band of Brønsted and Lewis acid sites is observed at 1482 cm^{-1}.

The activity of Zr-SBA-16 was probed as catalyst in one pot synthesis of dihydropyridine derivatives via Hantzsch reaction (Scheme 1) and the results are given in Table 2. In general, for similar amount of catalyst, the reaction went quicker with Zr-SBA-16(25) catalyst in 3 h compared to Zr-SBA-16(100) which took nearly 5.5 h. This observation is in line with acidity of these catalysts. Hence, further studies were carried out with Zr-SBA-16(25) catalyst.

No significant DHP yield was obtained when the reaction was performed under solventless conditions (Table 2,

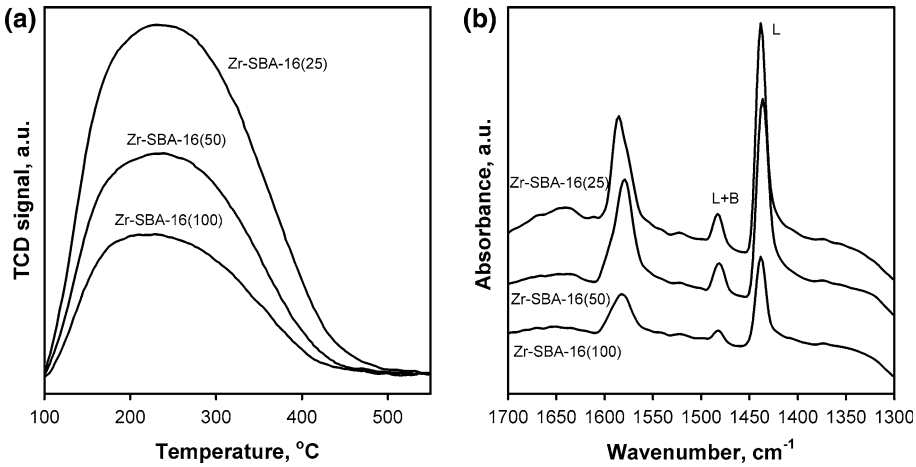

Fig. 5 **a** NH_3-TPD, **b** FTIR spectra of adsorbed pyridine of Zr-SBA-16 samples

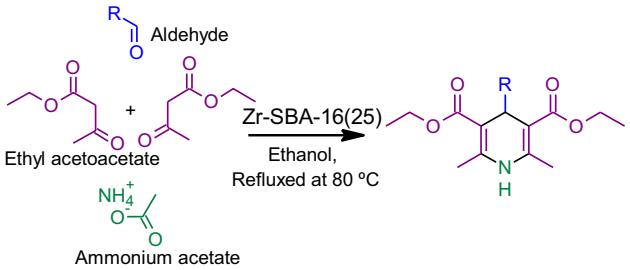

Scheme 1 Synthesis of DHP derivatives over Zr-SBA-16

entry 6). Probing various solvents, significantly higher yields of DHP in shorter reaction time was observed with polar protic solvents such as methanol and ethanol (Table 2, entries 1 and 2). On the other hand non-polar solvents such as hexane and polar aprotic solvents such as THF and acetonitrile gave poor yields of DHP (Table 2, entries 3–5). Moreover, with both substituted benzaldehydes and heterocyclic aldehydes the reaction went slightly faster with higher DHP yields compared to unsubstituted benzaldehyde (Table 2, entries 8–13). To emphasis the

Table 2 Effect of solvents and various substituted aldehyde in Hantzsch reaction at 80 °C

Entry	Aldehyde	Solvent	Time[a] (h)	Isolated yield (%)	Melting point (°C)
1	Benzaldehyde	Ethanol	3	77	159–160 [27]
2	Benzaldehyde	Methanol	4	74	
3	Benzaldehyde	Acetonitrile	7	59	
4	Benzaldehyde	THF	10	32	
5	Benzaldehyde	n-hexane	18	28	
6	Benzaldehyde	Solventless	24	Trace	
7	Benzaldehyde	Ethanol	12	10	
8	4-Bromobenzaldehyde	Ethanol	2	82	159–160 [28]
9	4-Chlorobenzaldehyde	Ethanol	2	89	148–149 [16]
10	4-Nitrobenzaldehyde	Ethanol	3	80	132–134 [16]
11	4-Methoxybenzaldehyde	Ethanol	2	87	160–161 [16]
12	Furan-2-carbaldehyde	Ethanol	2	90	159–160 [16]
13	Thiopene-2-carbaldehyde	Ethanol	2	94	165–167 [16]
14	Thiopene-2-carbaldehyde	Ethanol	6	47[b]	
15	Benzaldehyde	Ethanol	3	85	
16	Benzaldehyde	Ethanol	3	73	

Reaction conditions Zr-SBA-16(25) containing 0.06 mmol of Zr, substituted aldehyde (1 mmol), ethyl acetoacetate (2 mmol), ammonium acetate (1.2 mmol) and solvent (4 ml)

[a] Completion of the time monitored by TLC

[b] $ZrOCl_2$ was employed as catalyst (50 wt% with respect to total weight of substrates)

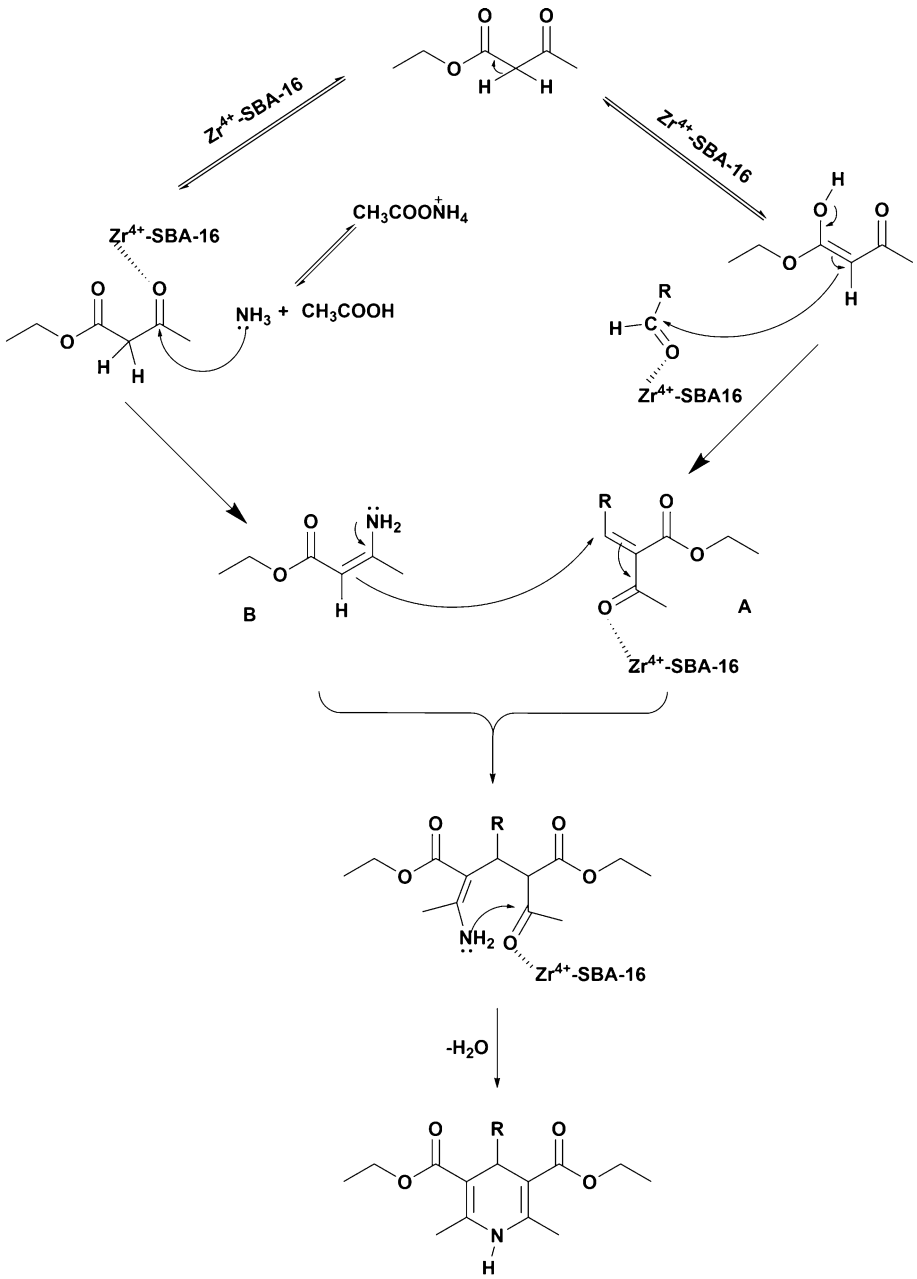

Scheme 2 Proposed mechanism for the formation of DHP products over Zr-SBA-16

activity of heterogeneous Zr-SBA-16, its activity is compared with homogeneous $ZrOCl_2$ under similar reaction conditions (Table 2, entry 14) which gave a yield of 47 % DHP even after 6 h of reaction time.

Catalysts were filtered off, washed with acetone and water and activated at 200 °C for 2 h and recycling of the catalyst investigations under similar reaction conditions (Table 2, entry 1), showed no appreciable decrease in isolated yield for two consecutive runs. However, after 4th recycle, the isolated yield decreased to 68 %, due to loss of catalyst (and active sites) in successive recycle runs.

The Hantzsch reaction is a typical Lewis acid catalyzed reaction [26] in which the synthesis of 1,4-dihydropyridines involves through two steps (Scheme 2). In the first step, the ethyl acetoacetate either can go Knoevenagel adduct formation from one equivalent of ethyl acetoacetate and benzaldehyde (intermediate A) or ester enamine formation from another one equivalent of ethyl acetoacetate with ammonia (intermediate B). Then from the subsequent cyclocondensation of both A and B takes place via Michael-type addition yielding the DHP as a second step.

Further the activity of Zr-SBA-16 is compared with ZrTUD-1, disordered mesoporous material and Zr-KIT-5,

cage type material (Table 2, entry 15 and 16) having similar Si/Zr ratio and the results suggest that Zr-KIT-5 performed slightly better than Zr-SBA-16 followed by ZrTUD-1. We propose that, the catalytic activity mainly depends on number and nature of acid sites. For instance, Zr-TUD-1 possessed a total acidity of 0.34 NH_3 mmol/g [22] whereas Zr-SBA-16 has a higher acid sites (0.55 NH_3 mmol/g). On the other hand, the total acidity of Zr-KIT-5 is very close to Zr-SBA-16 (0.59 NH_3 mmol/g) [19] and a higher activity of Zr-KIT-5 may be attributed to structural differences between SBA-16 and KIT-5, although further studies are needed to verify this hypothesis.

4 Conclusion

In conclusion, Zr was framework incorporated into SBA-16 cubic cage type ordered mesoporous silicate under acidic conditions employing F127 and n-butanol as a structure directing agents. Zr-SBA-16 materials were characterized and shown to possess highly ordered cubic cage type structure with high surface are and pore volume. Framework Zr^{4+} in tetrahedral coordination was evidenced from diffuse reflectance UV–Vis and FTIR studies. Zr-SBA-16 also possessed majorly Lewis acid sties stemming from Zr^{4+} incorporation that increased with Zr loading. Further, Zr-SBA-16 catalysts are shown to be active for Hantzsch synthesis of DHP derivatives in high yield in shorter reaction times.

References

1. A. Corma, S. Iborra, A. Velty, Chem. Rev. **107**, 2411 (2007)
2. E. Antonakou, A. Lappas, M.H. Nilsen, A. Bouzga, M. Stöcker, Fuel **85**, 2202 (2006)
3. J.S. Beck, J.C. Vartuli, W.J. Roth, M.E. Leonowicz, C.T. Kresge, K.D. Schmitt, C.T.W. Chu, D.H. Olson, E.W. Sheppard, S.B. Mccullen, J.B. Higgins, J.L. Schlenker, J. Am. Chem. Soc. **114**, 10834 (1992)
4. D. Zhao, J. Feng, Q. Huo, N. Melosh, G.H. Fredrickson, B.F. Chmelka, G.D. Stucky, Science **279**, 548 (1998)
5. F. Kleitz, T.-W. Kim, R. Ryoo, Langmuir **22**, 440 (2005)
6. E.M. Rivera-Muñoz, R. Huirache-Acuña, Int. J. Mol. Sci. **11**, 3069 (2010)
7. L. Zhao, Y. Dong, X. Zhan, Y. Cheng, Y. Zhu, F. Yuan, H. Fu, Catal. Lett. **142**, 619 (2012)
8. A.T. Shah, B. Li, Z.E.A. Abdalla, Microporous Mesoporous Mater. **130**, 248 (2010)
9. A.T. Shah, B. Li, Z.E. Ali, Abdalla. J. Colloid Interface Sci. **336**, 707 (2009)
10. R. Maheswari, M.P. Pachamuthu, A. Ramanathan, B. Subramaniam, Ind. Eng. Chem. Res. **53**, 18833 (2014)
11. A. Ramanathan, H. Zhu, R. Maheswari, P.S. Thapa, B. Subramaniam, Ind. Eng. Chem. Res. (2014). doi:10.1021/ie504386g
12. W. Yan, A. Ramanathan, M. Ghanta, B. Subramaniam, Catal. Sci. Technol. **4**, 4433 (2014)
13. J.M.R. Gallo, C. Bisio, L. Marchese, H.O. Pastore, Microporous Mesoporous Mater. **145**, 124 (2011)
14. N. Jiang, J.-B. Koo, S.-C. Han, S.-E. Park, Res. Chem. Intermed. **34**, 507 (2008)
15. M. Selvaraj, K. Shanthi, R. Maheswari, A. Ramanathan, Energy Fuels **28**, 2598 (2014)
16. A. Debache, W. Ghalem, R. Boulcina, A. Belfaitah, S. Rhouati, B. Carboni, Tetrahedron Lett. **50**, 5248 (2009)
17. C.A. Antonyraj, S. Kannan, Appl. Catal. Gen. **338**, 121 (2008)
18. M.P. Pachamuthu, V.V. Srinivasan, R. Maheswari, K. Shanthi, A. Ramanathan, Appl. Catal. Gen. **462–463**, 143 (2013)
19. A. Ramanathan, H. Zhu, R. Maheswari, B. Subramaniam, Chem. Eng. J. (2014). doi:10.1016/j.cej.2014.11.099
20. A. Ramanathan, M.C. Castro Villalobos, C. Kwakernaak, S. Telalovic, U. Hanefeld, Chem. Eur. J. **14**, 961 (2008)
21. A. Ramanathan, B. Subramaniam, R. Maheswari, U. Hanefeld, Microporous Mesoporous Mater. **167**, 207 (2013)
22. M.P. Pachamuthu, V.V. Srinivasan, R. Maheswari, K. Shanthi, A. Ramanathan, Appl. Catal. Gen. **462–463**, 143 (2013)
23. M.S. Morey, G.D. Stucky, S. Schwarz, M. Froba, J. Phys. Chem. B **103**, 2037 (1999)
24. B.L. Newalkar, J. Olanrewaju, S. Komarneni, J. Phys. Chem. B **105**, 8356 (2001)
25. Q. Pan, A. Ramanathan, W.K. Snavely, R.V. Chaudhari, B. Subramaniam, Ind. Eng. Chem. Res. **52**, 15481 (2013)
26. N. Koukabi, E. Kolvari, A. Khazaei, M.A. Zolfigol, B. Shirmardi-Shaghasemi, H.R. Khavasi, Chem. Commun. **47**, 9230 (2011)
27. P.P. Ghosh, S. Paul, A.R. Das, Tetrahedron Lett. **54**, 138 (2013)
28. A. Heydari, S. Khaksar, M. Tajbakhsh, H.R. Bijanzadeh, J. Fluor. Chem. **130**, 609 (2009)